

## Design and characterization of hybrid III–V concentrator photovoltaic–thermoelectric receivers under primary and secondary optical elements



T.K.N. Sweet<sup>a,\*</sup>, M.H. Rolley<sup>a</sup>, W. Li<sup>b</sup>, M.C. Paul<sup>c,\*</sup>, A. Johnson<sup>d</sup>, J.I. Davies<sup>d</sup>, R. Tuley<sup>e</sup>, K. Simpson<sup>e</sup>, F.M. Almonacid<sup>f</sup>, E.F. Fernández<sup>f</sup>, A.R. Knox<sup>c</sup>

<sup>a</sup> School of Engineering, Cardiff University, Cardiff CF24 3AA, UK

<sup>b</sup> School of Mathematics & Statistics, University of Glasgow, Glasgow G12 8SQ, UK

<sup>c</sup> School of Engineering, University of Glasgow, Glasgow G12 8QQ, UK

<sup>d</sup> IQE plc, St Mellons, Cardiff CF3 0LW, UK

<sup>e</sup> European Thermodynamics, Leicester LE8 0RX, UK

<sup>f</sup> University of Jaén, Jaén 23009, Spain

### HIGHLIGHTS

- Novel integration of III:V concentrator photovoltaic cells-thermoelectric modules.
- Optimized thermoelectric module geometry for cell temperature sensing and cooling.
- New III:V triple-junction cell six-parameter one-diode equivalent model developed.
- The model fitted experimental current–voltage data with a low 4.44% mean error.
- High combined primary & secondary optical intensity gain coefficient 0.92 obtained.

### ARTICLE INFO

#### Keywords:

Concentrator photovoltaic  
III:V triple-junction solar cell  
Thermoelectric  
Cell temperature  
Secondary optical element  
Optimization

### ABSTRACT

Lattice-matched monolithic triple-junction Concentrator Photovoltaic cells ( $\text{InGa}_{(0.495)}\text{P}/\text{GaIn}_{(0.012)}\text{As}/\text{Ge}$ ) were electrically and thermally interfaced to two Thermoelectric Peltier module designs. An electrical and thermal model of the hybrid receivers was modelled in COMSOL Multiphysics software v5.3 to optimize cell cooling whilst increasing photon energy conversion efficiency. The receivers were measured for current–voltage characteristics with the cell only (with sylguard encapsulant), under single secondary optical element at x2.5 optical concentration, and under Fresnel lens primary optical element concentration between x313 and x480. Measurements were taken in solar simulators at Cardiff and Jaén Universities, and on-sun with dual-axis tracking at Jaén University. The hybrid receivers were electrically, thermally and theoretically investigated. The electrical performance data for the cells under variable irradiance and cell temperature conditions were measured using the integrated thermoelectric module as both a temperature sensor and as a solid-state heat pump. The performance of six hybrid devices were evaluated within two 3-receiver strings under primary optical concentration with measured acceptance angles of  $1.00^\circ$  and  $0.89^\circ$ , similar to commercially sourced Concentrator Photovoltaic modules. A six-parameter one-diode equivalent electrical model was developed for the multi-junction cells under both primary and secondary optical concentration. This was applied to extract six model parameters with the experimental current–voltage curves of type A receiver at 1, 3 and 500 concentration ratios. Standard test conditions ( $1000 \text{ W/m}^2$ ,  $25^\circ \text{C}$  and Air Mass 1.5 Global spectrum) were assumed based on trust-region-reflective least squares algorithm in MATLAB. The model fitted the experimental current–voltage curves satisfactorily with a mean error of 4.44%. The combined primary and secondary optical intensity gain coefficient is as high as 0.92, in comparison with 0.50–0.86 for crossed compound parabolic concentrators. The determined values of diode reverse saturation current, combined series resistance and shunt resistance were similar to those

\* Corresponding authors.

E-mail addresses: [SweetT@Cardiff.ac.uk](mailto:SweetT@Cardiff.ac.uk) (T.K.N. Sweet), [Manosh.Paul@Glasgow.ac.uk](mailto:Manosh.Paul@Glasgow.ac.uk) (M.C. Paul).

of monocrystalline PV cell/modules in our previous publications. The model may be applicable to performance prediction of multi-junction CPV cells in the future.

## 1. Introduction

Concentrator photovoltaic (CPV) technology utilizes low cost glass/polymer optics to significantly increase direct normal irradiance (DNI) photon flux onto a small [typically  $5.5 \text{ mm} \times 5.5 \text{ mm}$ ] CPV cell. The optics concentrate sunlight and homogenise photon spectral distribution, significantly increasing cell efficiency. To maximize optical concentration two lenses are typically applied to CPV cells, a primary optical element (POE) and a secondary optical element (SOE). Modular CPV systems typically include dual-axis tracking systems to follow the sun's trajectory and maximize energy generation throughout the day.

CPV is a viable renewable energy technology for commercial-scale generation of solar electricity, with typically between  $\times 300$  and  $\times 1000$  optical concentration. The cumulative global installation capacity of CPV is currently greater than 370 MWp (December 2016) [1] with several power plants of  $\geq 30$  MWp capacity. These plants have been built in Golmud China, [Suncore, 60 MWp (2012) and 80 MWp (2013)], Touwsrivier, South Africa [Soitec, 44 MWp (2014)] and Alamosa, Colorado [Amonix, 30 MWp (2012)], with demonstrated reliability for over 7 years. For technical and economic viability annual DNI needs to exceed  $2000 \text{ kWh/m}^2$ , found in approximately 50% of global locations. A global map which represents the long-term average of daily/yearly global DNI is shown in Fig. 1 [2].

Compound semiconductor multi-junction CPV cells hold the highest world record cell efficiency at 46.0% [3], held by Fraunhofer ISE, Soitec and CEA-LETI [4]. CPV cells are structurally designed to minimize thermalisation and transmission losses. Multiple direct bandgap materials are epitaxially grown via metal organic vapour phase epitaxy (MOVPE) or molecular beam epitaxy (MBE). High purity III:V layers, with typical total epitaxial thickness of  $< 10 \mu\text{m}$ , have almost perfect crystallinity leading to low non-radiative losses in the CPV device. High extinction coefficients and anti-reflective coating of the cell enables effective absorption of incident solar photons in the wavelength range, 250–2500 nm. High charge carrier mobility and separation enables full-

spectrum energy harvesting. World III–V cell efficiency records have typically increased  $\sim 1\%$  per year over the past decade. Advanced modelling indicates realistic cell efficiency targets of greater than 50% (1000x concentration) by 2020 [5]. High-volume production cell efficiencies generally closely follow research trends. Recent techno-economic evaluation states that to compete with crystalline Silicon system, CPV system efficiency needs to reach 40% with cell efficiencies of 50% and module efficiencies of 44% [6].

Previous literature on first-generation Silicon PV cell technologies list the positive benefits of hybrid photovoltaic-thermoelectric performance, increasing the annual electricity yield of the lone PV module by 11–14.7% at  $25^\circ\text{C}$  [7]. There are only three research papers on III:V CPV cells integrated with thermoelectric (TE) technology. Two theoretical papers describe a GaAs/Ge PV-TE system providing a further 8% electrical efficiency relative to the lone PV technology [8]. Four PV technologies (compound Silicon, Copper Indium Gallium diselenide, Gallium Arsenide and a triple junction Gallium Indium Phosphide/Indium Gallium Arsenide/Germanium) were also theoretically modelled as part of a hybrid system [9]. For triple junction cell performance under 1-sun and higher concentrations, the hybrid device showed a larger system efficiency. One experimental reference paper detailed a hybrid III:V CPV-TE high system investigated under high optical concentration (approx.  $\times 200$ ) [10]. The hybrid produced more power than the PV alone at concentrations larger than  $\times 100$ , using the thermoelectric module as a generator in Seebeck mode.

The original work in this paper investigates the functionality and performance of novel hybrid CPV-TE receivers. The thermoelectric module is used as both an accurate cell temperature sensor (via  $V_{oc}$ ) and a heat pump in Peltier mode (upon application of current) for cell temperature control.

Domed-shaped single optical (SILO) lenses were used as the SOE for the receiver [11]. These optics also effectively encapsulate both the CPV cell and top electrical (n-type) contacts for protection against environmental conditions. The inevitable consequences of high irradiance

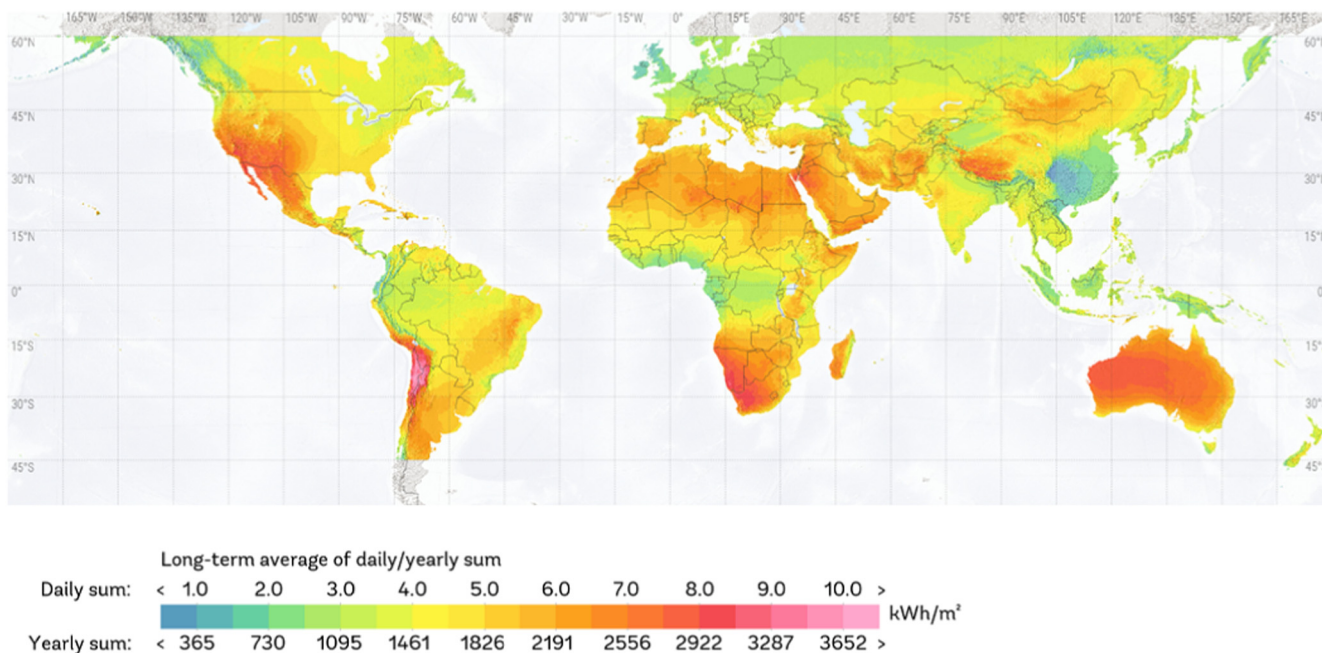


Fig. 1. Global resource map of direct normal irradiation. The solar resource is calculated by the Solargis model from atmospheric and satellite data with 10, 15 or 30-min time-steps. The effect of terrain are represented at a nominal spatial resolution of 250 m.

conditions are elevated cell temperatures and net power reduction. This is quantified by negative temperature coefficients for cell performance. The bandgap of each photon-absorbing layers is altered [12] reducing the cell voltage and slightly increasing photo-generated current at higher temperatures. Active solid-state cooling of the CPV cell increases the power output and potentially reduces thermal degradation of the III-V compound semiconductor cell. This becomes an important consideration when moving to higher optical concentrations to drive to lower levelised costs of energy.

A Closed Loop Integrated Cooler (CLIC) with temperature reference chip (Temp IC) was developed for additional temperature data in [13]. An AUTOLAB potentiostat system was also used for the I–V data acquisition in the experiments conducted inside a Faraday cage to eliminate any ambient light effects [14]. The POE was optimized using the Helios 3198 solar simulator at the University of Jaén [15]. A Delta Elektronika SM120-13 power supply unit was used to obtain the I–V measurements at the University of Jaen. A sensor based on the III–V material isotype solar was used to characterize the spectrum [16], and a solar spectral irradiance meter was applied to record the spectral direct normal irradiance under outdoor conditions for multi-junction cell based CPV modules [17].

Modelling multi-junction cell/module is another important task in

design and characterization of CPV systems. For multi-junction PV cells/modules, there appears to be two methods for describing their I–V curves, i.e. (1) sub-cells model method, and (2) global model method. In the sub-cells model, the multi-junction cells/modules are divided into a few sub-cells, for example, for a triple-junction cell, its subcells include top-, middle- and bottom-cells connected in series by tunnel junctions. These three sub-cells have their own I–V curves to contribute the global I–V curve according to the Kirchoff’s rules. Detailed I–V curves of a multi-junction PV cell/module show a variety in shape and pattern, depending on the cell/module design configuration and material properties, and usually can be determined by using a complex photon quantum calculation in terms of the terrestrial solar spectrum and cell geometry [18]. An analytical method for translating I–V curves of series-connected multi-junction solar cells was presented and the effects of irradiance, cell temperature and spectral variations were measured [19]. The complex photon quantum calculation was involved to estimate the electrical performance of multi-junction cells [20]. A theoretical analysis of the impact of atmospheric parameters on the spectral, electrical and thermal performance of a concentrating III–V triple-junction solar cell was carried out in [21].

In sub-cell models, once the short-circuit currents and open circuit voltages of the sub-cells are known, their 7 (two-diode model) [22], 8,

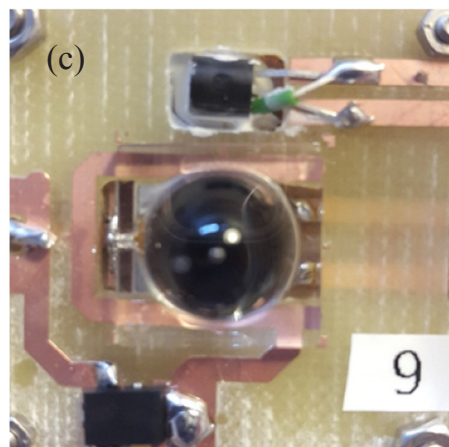
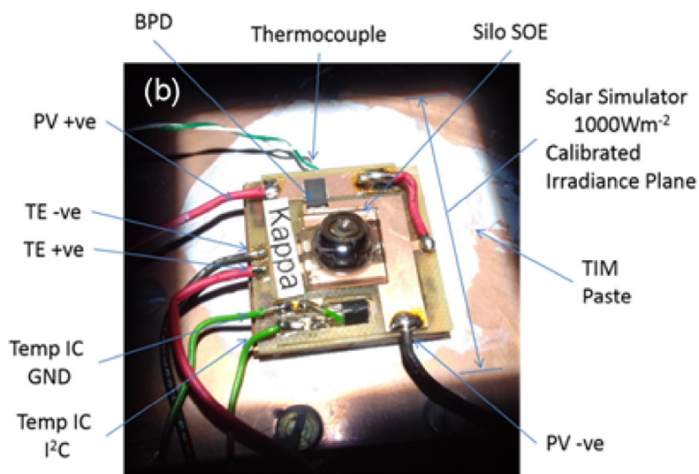
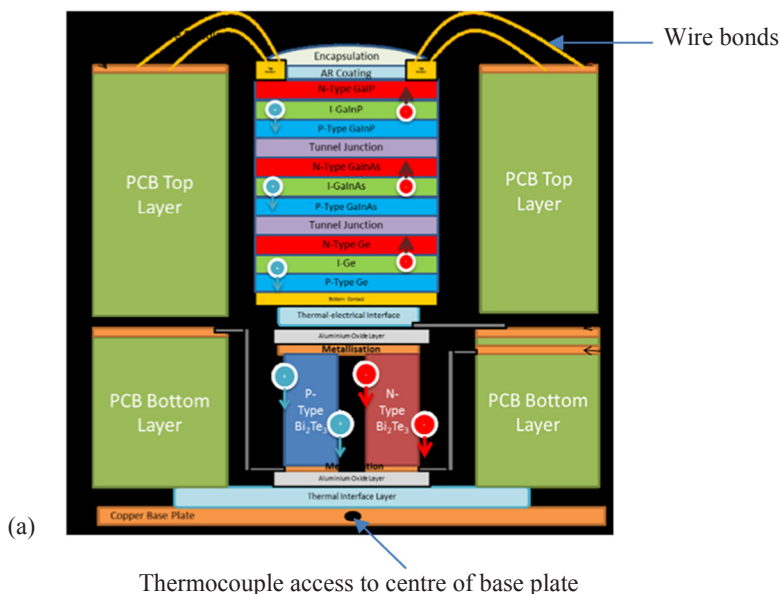


Fig. 2. (a) CPV-TE hybrid receiver PCB architecture [15] (b) Type A “Kappa” SOE-CPV-TE hybrid receiver overview (c) Type B SOE-CPV-TE receiver number 9.

[23], 10 (one-diode model) [22], or 24 [24] model parameters can be decided by making use of the measured global  $I$ - $V$  curves [25]. In the global model, a multi-junction cell/module is no longer divided into a few sub-cells, instead is simplified to one equivalent electrical model [26] to reduce the number of model parameters in a great deal [27]. These model parameters can be decided by experimental global  $I$ - $V$  curves.

In the paper, the novel hybrid receivers were designed, but also electrically and thermally measured under different cell temperature conditions. Standard test conditions (STC) of  $1000 \text{ W/m}^2$  irradiance,  $25^\circ\text{C}$  temperature and AM1.5G/D spectrum conditions gave baseline cell performance data. The experimental  $I$ - $V$  curves of type A receivers at 1, 3 and 500 concentration ratios were represented by making a proposed six-parameter equivalent single-diode electrical model. The six model parameters were extracted from the curves based on the trust-region-reflective least squares algorithm in MATLAB. The determined parameters were contrasted with those of the monocrystalline PV cell/modules with crossed compound parabolic concentrators (CCPC) in existing papers.

From the modelling context, the paper further exhibits the novelty of the proposed six-parameter single-diode equivalent electrical model for the multi-junction PV cells/modules, particularly, the power function for the optical gain of a multi-junction cell with SOE only, or with both SOE and POE at a geometrical concentration ratio ( $CR$ ) as high as 500.

## 2. Experimental

The hybrid receivers were manufactured using standard cleanroom and wire-bonding techniques. The architecture of the hybrid device shown in Fig. 2(a) [12] includes two active components. A  $5.5 \times 5.5 \text{ mm}$  lattice-matched triple junction solar cell. These cells were bonded to a pre-metallised Marlow CM23-1.9 bismuth telluride TE module, in receiver type A, see schematic Fig. 2(b) “Kappa”. The hybrid CPV cell-thermoelectric module hybrid receiver was modelled and re-designed for operation at x300 concentration. Modules were supplied by European Thermodynamics for receiver types B and C. The primary aim was to keep the cell temperature below the manufacturer’s high temperature limit of  $85^\circ\text{C}$ . The thermal contact between the CPV cell and the TE module was improved by changing the thermal interface material and by reducing its thickness for receiver types B and C. The CPV cells used in the hybrid receivers were from the same

manufacturer, but from three different wafers/growth campaigns. A photograph of receiver type C, with improved PCB design to reduce the likelihood of hot-spot formation, is presented as Fig. 2(c). A water heat exchanger and appropriate thermal interface material (TIM) was used in all indoor solar simulator experiments. Temperature measurements were taken at the TE cold-side and ambient temperature using a K-type thermocouple, in conjunction with a Fluke 52II thermometer. A Closed Loop Integrated Cooler (CLIC) and temperature reference chip (Temp IC) were used for additional temperature data as reported in previous work [13]. A forward looking infrared camera (FLiR i7) was used for thermal imaging distribution measurements.

At Cardiff University a LCS-100 Class ABB (ASTM, IEC and JIS standards) solar simulator, with the  $1000 \text{ W/m}^2$  calibrated irradiance plane found using a Kipp and Zohan CMP11 pyranometer, was used for STC current-voltage ( $I$ - $V$ ) scans. An AUTOLAB potentiostat system was used for  $I$ - $V$  data acquisition, and the experiments were conducted inside a Faraday cage to eliminate any ambient light effects [14]. Steady-state temperatures of  $25 \pm 1^\circ\text{C}$  were achieved, prior to measuring CPV cell  $I$ - $V$  curves. This was to minimize electrical output changes due to the temperature coefficients of the cell. The current-voltage graphs for type B receivers are presented in Fig. 3. Measurement uncertainties for the experimental equipment used are presented in Table 1 and CPV cell and CPV-TE module characterization data are given in Table 2.

The SOE CPV-TE hybrid receivers [14] were connected in two series-connected strings of three receivers, matched via maximum power point current ( $I_{\text{mpp}}$ ) values. The primary optical elements, designed to give x313 concentration ratio, were added to the module. To protect the connecting wires and temperature sensitive devices on the hybrid receivers, off-axis shield was added to reflect back solar irradiation using 3M Reflectec film. High-temperature kapstan tape was used to secure the film.

The vertical distance of the POE was optimized using the Helios 3198 solar simulator from Solar Added Value Company at the CEAEMA in the University of Jaén [15]. A Delta Elektronika SM120-13 power supply unit was used to obtain the  $I$ - $V$  measurements at the University of Jaen. This solar simulator uses a Xenon flash lamp for simulating the solar radiation and a parabolic mirror as a collimator. The spectral irradiance distribution can be tuned to match the AM1.5D reference spectrum by using appropriate filters, and the collimation angle is around  $\pm 0.3^\circ$ . Also, the Spectra Matching Ratio (SMR) for the top and middle sub-cells was monitored through the measurements of

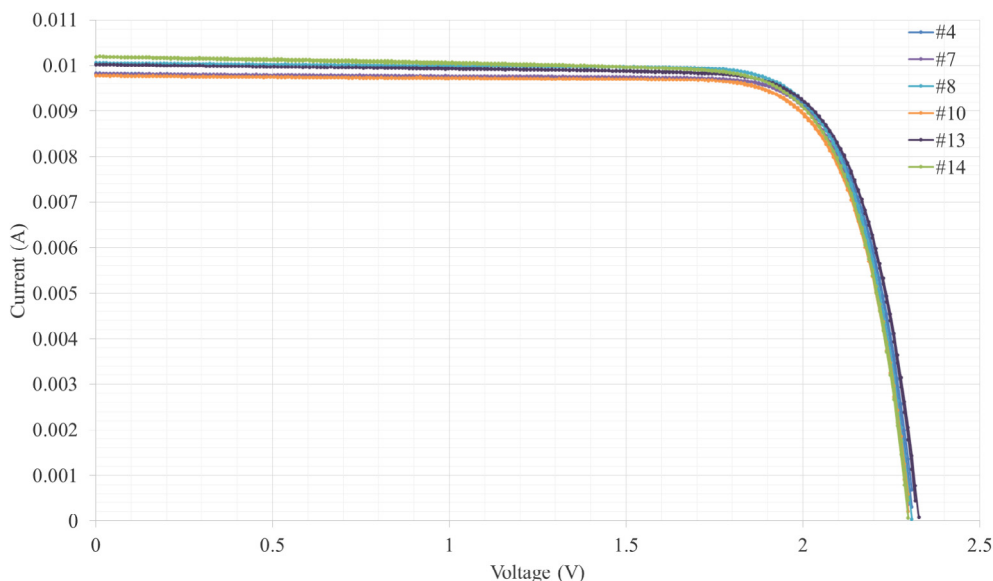


Fig. 3. Current-Voltage curves for type B receivers.

**Table 1**  
Equipment measurement uncertainties.

Equipment	Resolution	Interval	Range of reading	Uncertainty	Other
Autolab	I 6E–6 A V 0.3E–6 V	3E–7 A 0.15E–6 V	± 2A ± 10 V	Accuracy ± 0.2%	
Pyranometer (Kipp & Zonen CMP11)	A 5.12 μV/W/m <sup>-2</sup> A 8.89 μV/W/m <sup>-2</sup> A 9.01 μV/W/m <sup>-2</sup>	2.56 μV/W/m <sup>-2</sup>	285–2800 nm	Temperature change < 1% Time change < 5 s	Range –40 to 80 °C 4000 W/m <sup>2</sup> max
Spectroradiometer Silicon reference Cell seaward solar survey 100)	1 nm 1 Wm <sup>-2</sup>	0.5 nm 0.5 Wm <sup>-2</sup>	24–800 nm 100–1250 Wm <sup>-2</sup>	± 2 °C stability	Range –10 to 40 °C 1 °C ± 0.5 °C resolution
FLiR i7 camera	0.1 °C	0.05 °C	Range –20 to 250 °C		9 Hz, 75–13 μm detection
IR thermometer (Maplin TN439L0)	3 °C	1.5 °C	Range –25 to 265 °C		Area 0.08 m <sup>2</sup> @ 0.6 m Distance 0.13 m <sup>2</sup> @ 1 m
Thermocouples (K type, PTFE 1 m)	3 °C	1.5 °C	Range –75 to 250 °C		
Thermocouples reader (Fluke 52)	0.1 °C	0.05 °C	0–9999 °C		Thermocouple dependant
Multimeter (Chauvin Arnoux)	V 0.01 mV 0.1 Ohms	0.005 mV 0.05 Ohms	0–1000 V 0–60 MOhms		

component cells to ensure the adequate input spectrum. This type of light source has a small time period for each measurement (< 2 ms). It is effective for large area testing, without need for a continuous light source or temperature control of the receiver. The configuration of SOE-CPV-TE receivers is given in Fig. 4(b).

The samples were located using a right-angle clamp from Thor labs, then the focal length distance was adjusted until the light spot of the POE was incident on the fulcrum of the SOE. When locating the samples

within the clamp, type B receivers were more compatible in size than type A. This had the potential to introduce rotational inaccuracies for the type A receivers. This POE alignment procedure introduced a systematic error between the obtained I–V traces. However, the data obtained was comparable to experiments using the type B receivers both outdoors in the module, under POE, and indoors as receivers under SOE only.

After optical alignment, the acceptance angle of each string was

**Table 2**  
CPV-TE hybrid receiver pre-manufacture cell and thermoelectric device data.

Receiver			Wafer	Cell	Thermoelectric module			
ID	Type	Optics	ID	ID	Batch	ID	RAC (Ohms)	Thick (mm)
Kappa	A	SOE	#0556	48	CM23-1.9		1.23	1.63 + metallization
Lambda	A	No	#0556	40	CM23-1.9			
4	B	SOE	#2047	74	2,484,935	4	1.98	2.360
7	B	SOE	#2047	48	2,484,935	7	1.93	2.410
8	B	SOE	#2047	67	2,484,935	8	2.08	2.400
10	B	SOE	#2047	47	2,484,935	10	1.99	2.410
13	B	SOE	#2047	93	2,484,935	13	1.99	2.510
14	B	SOE	#2047	119	2,484,935	14	1.89	2.480
21	C	No	#4853	49	2,484,935	21	1.95	2.362
22	C	No	#4853	61	2,484,935	22	1.97	2.422
23	C	No	#4853	26	2,484,935	23	1.88	2.484
24	C	No	#4853	39	2,484,935	24	1.88	2.553
25	C	No	#4853	27	2,484,935	25	1.96	2.485
26	C	No	#4853	80	2,484,935	26	1.98	2.544
30	C	SOE	#4853	36	2,484,935	30	2.02	2.474

Receiver	1-sun data					330-sun data				
ID	I <sub>sc</sub> (mA)	V <sub>oc</sub> (V)	P <sub>m</sub> (mW)	FF (%)	η <sub>eff</sub> (%)	I <sub>sc</sub> (A)	V <sub>oc</sub> (V)	P <sub>m</sub> (W)	FF (%)	η <sub>eff</sub> (%)
Kappa	4.47	2.26	8.30	82.2	27.4	1.528	2.7994	3.496	81.7	33.8
Lambda	4.44	2.28	8.59	84.9	28.4	1.521	2.8203	3.502	81.6	33.8
Mean	4.46	2.27	8.45	83.6	27.9	1.524	2.81	3.499	81.65	33.8
4	4.50	2.19	7.62	77.4	25.2	1.474	2.81	3.402	82.3	34.3
7	4.50	2.16	7.65	78.7	25.3	1.469	2.79	3.334	81.4	33.8
8	4.52	2.19	7.71	78.0	25.5	1.473	2.79	3.379	82.2	34.3
10	4.52	2.16	7.54	77.2	24.9	1.479	2.80	3.374	81.4	34.1
13	4.48	2.19	7.72	78.6	25.5	1.462	2.81	3.373	81.9	34.2
14	4.48	2.17	7.66	78.6	25.3	1.458	2.79	3.311	81.4	33.6
Mean	4.50	2.18	7.65	78.1	25.3	1.469	2.80	3.362	81.77	34.05
21	4.14	2.49	8.76	85.0	28.9	1.384	2.86	3.368	85.2	33.3
22	4.15	2.49	8.60	83.4	28.4	1.379	2.86	3.348	84.7	33.3
23	4.13	2.49	8.55	83.2	28.3	1.390	2.85	3.364	84.8	33.1
24	4.14	2.49	8.53	82.7	28.2	1.384	2.85	3.351	84.9	33.1
25	4.13	2.50	8.68	84.1	28.7	1.389	2.86	3.379	85.2	33.2
26	4.14	2.49	8.75	84.9	28.9	1.379	2.87	3.353	84.6	33.3
30	4.12	2.51	8.75	84.5	28.9	1.388	2.85	3.373	85.3	33.1
Mean	4.14	2.49	8.66	84.0	28.6	1.385	2.86	3.362	85.0	33.2

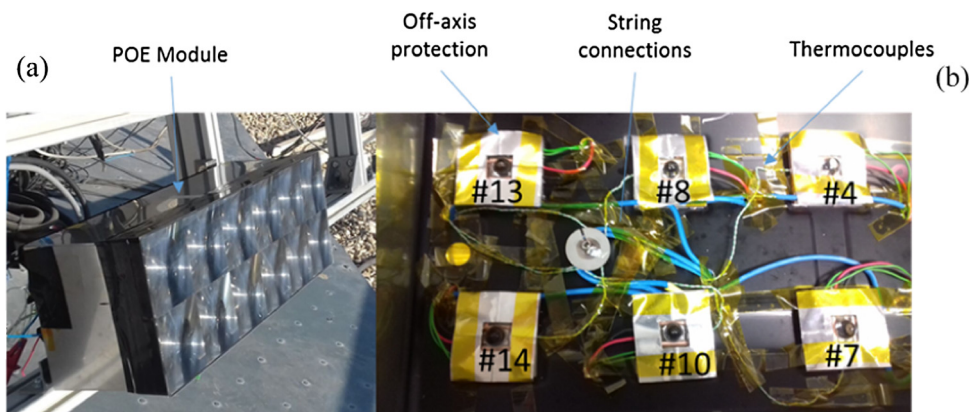


Fig. 4. CPV-TE module on-sun (a) and overview of the SOE-CPV-TE receivers (b) at Jaén University.

measured with the Helios 3198 CPV solar simulator at the CEAEMA in the University of Jaen as a quadrant of the module. Q1 for receivers #13 and #8 and Q4 for receivers #10 and #7. STC conditions were used,  $1000 \text{ W/m}^2$ , spectral irradiance similar to AM1.5D reference spectrum,  $\text{SMR (top/mid)} = 1 \pm 0.05$  and room temperature of  $25 \text{ }^\circ\text{C} \pm 0.5 \text{ }^\circ\text{C}$ . The optimum alignment was considered at the point 0 of the x-axis. The values obtained were  $1.00^\circ$  (string A, 13, 8 & 4) and  $0.89^\circ$  (string B, 14, 10 & 7), given in Fig. 5. The results are comparable to most commercial modules.

The module was mounted on a high-precision dual-axis tracker from BSQ Company located on the rooftop of the CEAEMA, with a known mis-alignment of within  $0.2^\circ$  accuracy, is shown in Fig. 4(a) [15]. The measurement setup at CEAEMA, Jaén University, included an atmospheric station MTD 3000 from Geonica Company to record the main atmospheric parameters. This station incorporates a pyrheliometer and various pyranometers to measure different components of the irradiance (i.e. global horizontal and normal, direct normal and diffuse horizontal). It also includes several sensors to record other crucial parameters such as air temperature, wind speed and direction or relative humidity. Also, the centre is equipped with a sensor based on III–V material isotope solar cells from Black Photon Company to characterize the spectrum and a solar spectral irradiance meter (SolarSIM-D2) from Spectrafy Inc. to record the spectral direct normal irradiance among other key parameters for the outdoor spectral characterization of multi-junction based CPV modules such as aerosol optical depth at  $550 \text{ nm}$  (AOD550) [16] or precipitable water (PW) [17]. An IV tracer was used to evaluate CPV cell performance of all three receivers within each string. The rear substrate temperature for all of the receivers were recorded during I–V scans using thermocouples and two Picologger TC-08s. Three power supplies were used to supply the excitation current to the TEM during testing. A schematic of the setup is given in Fig. 6.

Type C receivers 21, 22, 23, 24, 25, 26, detailed in Table 2, were manufactured for I–V and accelerated lifetime testing. Receiver 30 had a SILO SOE attached to the cell with Sylguard encapsulant. The optical concentration of the SOE was calculated with respect to  $I_{sc}$  as  $\times 2.57$ . The data is presented as Fig. 7. Comparative measurements were performed on type A “Kappa” and type B receiver #13 under SOE at Cardiff University and SOE + POE at Jaén University, see Fig. 8. Under 1-sun conditions, measured under SOE, the  $V_{oc}$  of “Kappa” was  $0.1 \text{ V}$  higher than that of receiver #13, indicating  $\sim 25\text{--}30 \text{ }^\circ\text{C}$  lower cell temperature for Kappa. The  $I_{sc}$  of #13 was  $0.02 \text{ A}$  higher than Kappa when measured under POE, consistent with a lower cell temperature for Kappa.

The current–voltage characteristics of type B hybrid receivers were measured under primary optical concentration in the solar simulator at CEAEMA, the results are presented as Fig. 9 and Table 3. In comparison with CPV cell probe measurements, based on the  $I_{sc}$  data, the concentration ratio under the POE optics was  $\times 371$  for Kappa (type A) and  $\times 375$  for receiver #13 (type B).

The type B CPV-TE hybrid receiver #9 was measured for current–voltage characteristics with a temperature range of  $5\text{--}80 \text{ }^\circ\text{C}$ . The module was used to accurately measure and control operational CPV cell temperature and the I–V results are presented in Fig. 10(a). The decrease in  $V_{oc}$  and  $V_{mpp}$  with temperature increase is highly linear ( $R^2$  0.983 & 0.972), see Fig. 10(b). The temperature coefficients are  $-0.00255$  and  $-0.00221 \text{ V/K}$ . The increase in  $I_{sc}$  and  $I_{mpp}$  with temperature increase is linear ( $R^2$  0.754 & 0.880), see Fig. 10(c). The temperature coefficients are  $0.00049$  and  $0.00048 \text{ A/K}$ . The temperature coefficient for CPV cell efficiency was calculated as  $-0.055\%/K$ . The trend was highly linear ( $R^2$  0.957) over the  $75 \text{ }^\circ\text{C}$  temperature range tested, see Fig. 10(d).

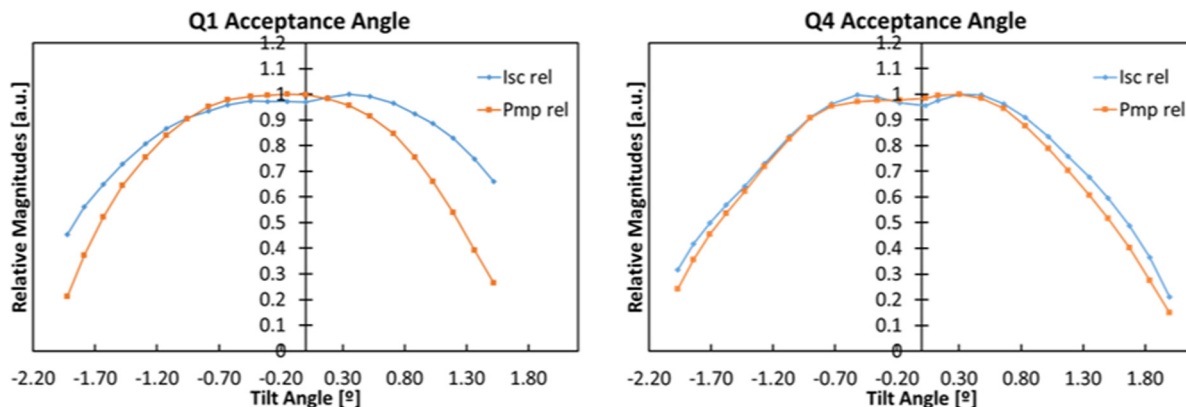


Fig. 5. Acceptance angle data for quadrants 1 and 4 of the type B CPV-TE hybrid module.

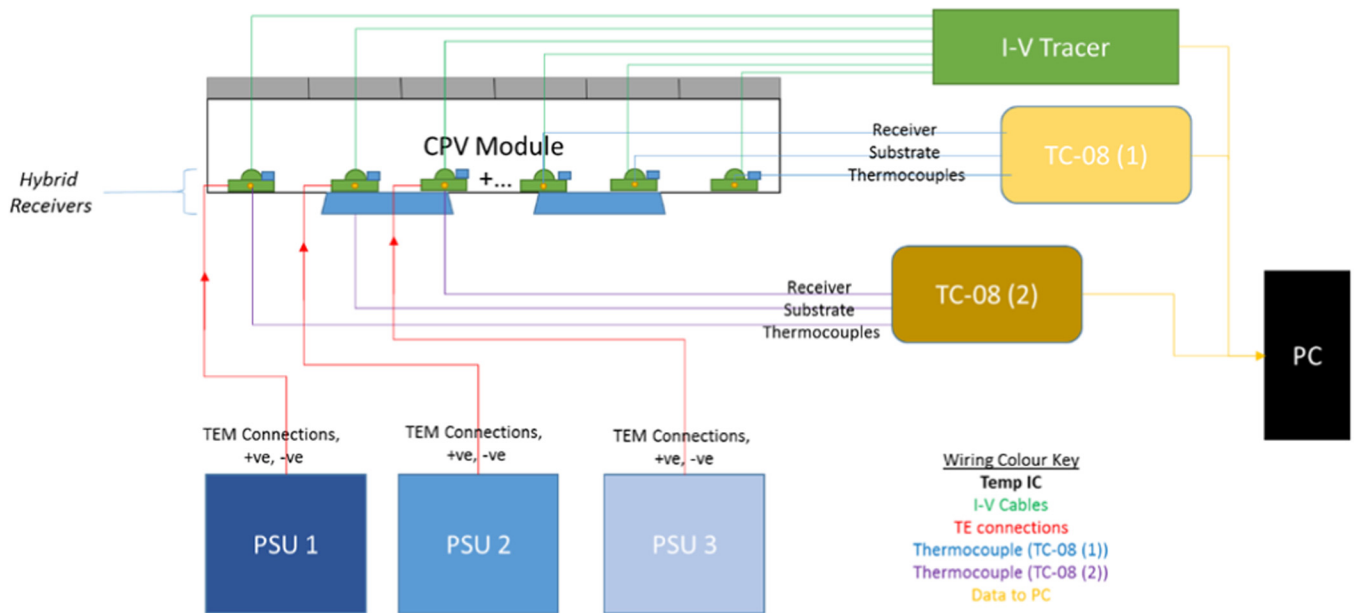


Fig. 6. Metrology of the on-sun POE-SOE-CPV-TE receiver module at Jaén University.

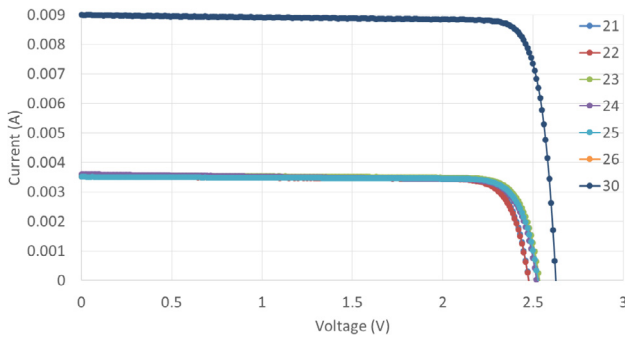


Fig. 7. Type C receiver I–V plots without SOE (21–26) and with SOE optics (30) for accelerated lifetime testing.

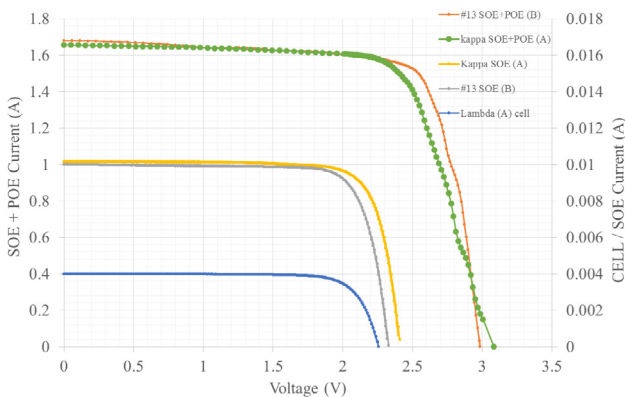


Fig. 8. I–V data for type A “Lambda” and “Kappa” and type B “13” receivers.

### 3. Thermoelectric cooler model

An electrical and thermal model of the thermoelectric module, linked to a thermal model of the PV cell was produced in the finite element analysis program COMSOL Multiphysics 5.3. The thermal impact of the SOE was not included as much of the initial fitting was performed without the SOE. Whilst the SOE will enhance the heat loss through the additional surface area available for convection, the heat conduction through the thermoelectric cooler (TEC) will be the

dominant cooling mechanism. The TEC model was matched against specifications given in the datasheet, and thermal interface properties were determined by fitting to experimental data on cell temperature at x70 optical concentration. Without any further fitting, this model then gave good fits to the TEC IV, the PV cell temperature vs TEC current and TEC current required to maintain 25 °C and 50 °C at 0–1000 W/m<sup>2</sup> illumination. This modelling allowed the key challenges of the thermal design of type A to be identified, shown graphically in Fig. 11. This indicates that very high temperatures may be experienced by the type A design under x300 optical concentration, due to the temperature drop across the PV cell to TEC interface, and the TEC itself. Type B was predicted to have a much lower operating temperature, due to the improvement of the PV cell to TEC interface and the improved thermal conductance of the TEC module, predominantly by increasing its area.

### 4. Electrical model parameters

Based on experimental I–V results, adding the SOE and POE have demonstrated a considerable improvement in the receiver electrical performance, especially in the current under STC. To characterize the favorable effect of SOE and POE on I–V curves quantitatively, we will add geometrical CR of SOE and POE into the current–voltage electrical model of the multi-junction modules presented in the paper, and extract SOE and POE optical intensity gain coefficients and the corresponding model parameters. Since the single-junction like method mentioned in the introduction is simpler and with a less number of parameters, it might potentially be applied in operational management of concentrating multi-junction PV cells/modules/arrays. This method is adopted in the paper.

#### 4.1. Electrical model equation

For a multi-junction cell/module with SOE and POE, its complex internal electrical circuits can be represented by a lumped one-diode equivalent electrical circuit model, as shown in Fig. 12. Here the optical unit composed of POE and SOE is added on the top of the bare/flat PV cell. In this case, the mathematical expression for this equivalent circuit is written as [18]

$$I = I_{ph} - I_d \left[ \exp \left\{ \frac{q(V + R_s I)}{nkT} \right\} - 1 \right] - \frac{V + R_s I}{R_{sh}} \quad (1)$$

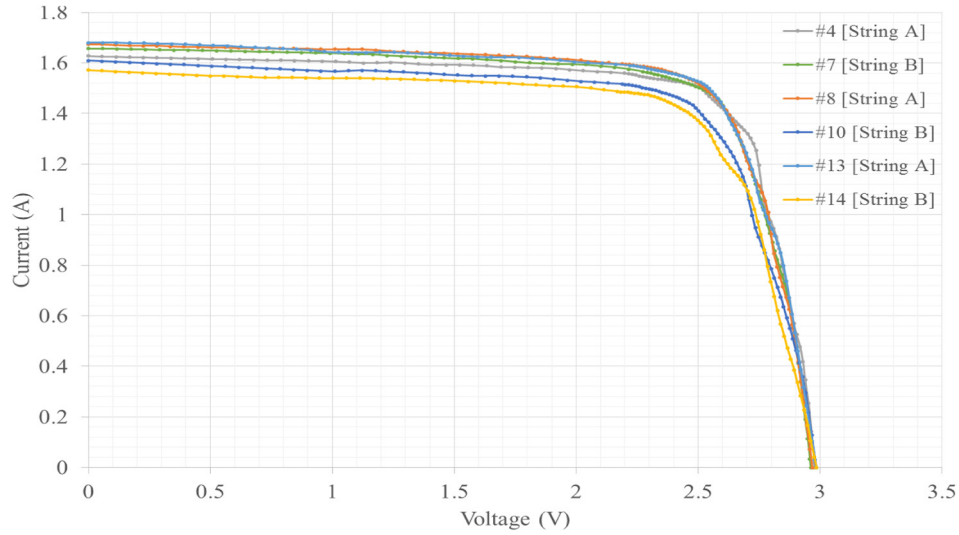


Fig. 9. Type B CPV-TE hybrid receivers tested under POE solar simulator at CEAEMA.

Table 3

Hybrid POE-SOE-CPV-TE receiver test data measured at CEAEMA.

Receiver	373-sun data					
	$I_{sc}$ (A)	$V_{oc}$ (V)	$P_m$ (W)	FF (%)	$\eta_{eff}$ (%)	SMR
Kappa	1.66	3.1	3.6	71	21.4	1.00
4	1.63	3.0	3.8	78	22.3	1.01
7	1.66	3.0	3.8	77	22.3	1.01
8	1.67	3.0	3.8	76	22.5	1.01
10	1.61	3.0	3.6	74	21.0	1.01
13	1.68	3.0	3.8	76	22.6	1.01
14	1.59	3.0	3.5	74	20.7	1.01
Mean	1.64	3.0	3.72	75.8	21.9	1.01

in which  $V$  and  $I$  are the output voltage and current of the PV cell/module respectively,  $q$  is the electron charge,  $q = 1.60217646 \times 10^{-19}$  C, and  $k$  is the Boltzmann constant,  $k = 1.38065031 \times 10^{-23}$  J/K,  $T$  is the cell temperature,  $I_d$  is the diode reversal saturation current,  $n$  is the diode quality factor, i.e. ideality factor,  $R_s$  is the combined series resistance and  $R_{sh}$  is the shunt resistance.  $I_{ph}$  is the photo current and depends on both radiation intensity  $S$  and cell temperature  $T$ . In the model Eq. (1), five variables such as  $I_{ph}$ ,  $I_d$ ,  $n$ ,  $R_s$  and  $R_{sh}$  are the model parameters and need to be determined with an experimental  $I$ - $V$  curve at STC ( $S = 1000$  W/m<sup>2</sup>,  $T = 25$  °C).

Following the idea in [28], the SOE or POE or both are regarded as an optical intensity amplifier with a gain coefficient,  $m$ , such that the photo current, increased by the POE and SOE, is presented in terms of a power function of total concentration ratio and gain coefficient as follows

$$I_{ph} = CR^m I_{ph0} \quad (2)$$

Substituting Eq. (2) into Eq. (1), the  $I$ - $V$  curve equation for the multi-junction PV cell/module with SOE or POE or both at STC is written as

$$I = CR^m I_{ph0} - I_d \left[ \exp \left( \frac{q(V + R_s I)}{nkT} \right) - 1 \right] - \frac{V + R_s I}{R_{sh}} \quad (3)$$

Note that for the case without POE and SOE,  $CR = 1$ , Eq. (3) can restore the case without either SOE or POE. Eq. (3) represents a six-parameter lumped electrical model for a multi-junction PV cell/module with SOE or both SOE and POE at STC. Six parameters,  $I_{ph0}$ ,  $I_d$ ,  $n$ ,  $R_s$ ,  $R_{sh}$  and  $m$  in Eq. (3) need to be determined based on the experimental  $I$ - $V$  curves under three conditions; the first one for a PV cell/module without SOE or POE, the second one for the same PV cell/module with SOE, and the third condition for the same PV cell/module with both

POE and SOE.

#### 4.2. Method for determining six parameters

The trust-region-reflective (TRR) least squares algorithm provided in MATLAB [29] is employed to optimize the following objective function for the six parameters

$$f(I_{ph0}, I_d, n, R_s, R_{sh}, m) = \sum_{i=1}^{N_1} [(I_{1i} - I_{1i}^{exp})/I_{sc1}^{exp}]^2 + \sum_{i=1}^{N_2} [(I_{2i} - I_{2i}^{exp})/I_{sc2}^{exp}]^2 + \sum_{i=1}^{N_3} [(I_{3i} - I_{3i}^{exp})/I_{sc3}^{exp}]^2 \rightarrow \min \quad (4)$$

where  $N_1$ ,  $N_2$  and  $N_3$  are the numbers of experimental data of  $I$ - $V$  curves without optical unit, with SOE, with both SOE and POE, respectively;  $I_{1i}$ ,  $I_{2i}$  and  $I_{3i}$  are the currents calculated from Eq. (3) with a set of temporary six parameters at the  $i$ th experimental voltages  $V_{1i}^{exp}$ ,  $V_{2i}^{exp}$  and  $V_{3i}^{exp}$  in the cases without optical unit, with SOE, and with SOE and POE, respectively;  $I_{1i}^{exp}$ ,  $I_{2i}^{exp}$  and  $I_{3i}^{exp}$  are the currents at the  $i$ th experimental voltages accordingly. The validation of the algorithm has been made in [28].

Once a set of six parameters are decided, the maximum electrical power will be tracked by minimizing the following objective function with the same optimization algorithm as above

$$f(I_{max}, V_{max}) = \frac{1}{IV} \rightarrow \min \quad (5)$$

where  $I_{max}$  and  $V_{max}$  respectively are the current and voltage at which a maximum electrical power,  $P_{max}$ , is achieved.

#### 4.3. Extracted six parameters

The six parameters of the PV cell were extracted based on its  $I$ - $V$  curves presented in Fig. 8 under  $CR = 1, 3$  and 500 in the cases for bare cell, with SOE only and with both SOE and POE. To assess the error in  $I$ - $V$  curve fittings, the following errors are defined;

$$\begin{cases} \varepsilon = \frac{1}{3}(\varepsilon_1 + \varepsilon_2 + \varepsilon_3) \\ \varepsilon_1 = \sqrt{\frac{\sum_{i=1}^{N_1} [(I_{1i} - I_{1i}^{exp})/I_{sc1}^{exp}]^2}{N_1}} \times 100\% \\ \varepsilon_2 = \sqrt{\frac{\sum_{i=1}^{N_2} [(I_{2i} - I_{2i}^{exp})/I_{sc2}^{exp}]^2}{N_2}} \times 100\% \\ \varepsilon_3 = \sqrt{\frac{\sum_{i=1}^{N_3} [(I_{3i} - I_{3i}^{exp})/I_{sc3}^{exp}]^2}{N_3}} \times 100\% \end{cases} \quad (6)$$

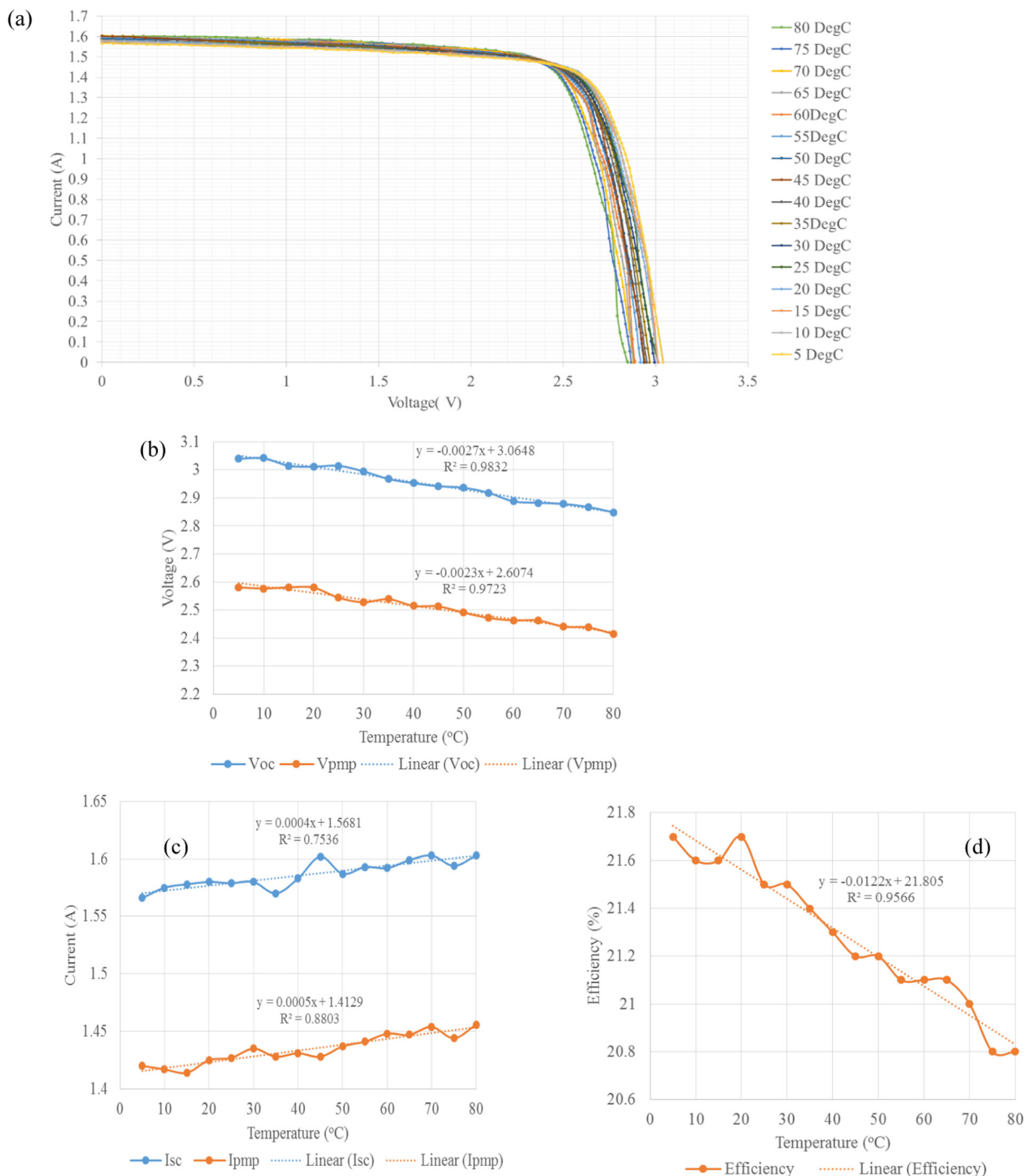


Fig. 10. I–V curve plots of receiver “9” (B) in 5 °C temperature steps (a).  $V_{oc}$  and  $V_{mpp}$  vs temperature curve (b).  $I_{sc}$  and  $I_{mpp}$  vs temperature curve (c) and CPV cell efficiency vs temperature curve (d).

where  $\epsilon_1$ ,  $\epsilon_2$  and  $\epsilon_3$  are the mean errors when the multi-junction cell is without any optical elements, with SOE only, and with both SOE and POE,  $\epsilon$  is the arithmetic mean error of  $\epsilon_1$ ,  $\epsilon_2$  and  $\epsilon_3$ .

Table 4 presents the range of six parameters during the parameter optimization process and their extracted values. For comparison, the extracted six parameters for monocrystalline PV cell with 1 CCPC, and monocrystalline PV modules respectively with  $2 \times 2$ ,  $9 \times 9$  CCPC in [28] are involved. A comparison of the predicted I–V curves is made against with the experimental I–V curves of type A in Fig. 13. The predicted I–V curves are basically in good agreement with the measurements with a mean error in current of 4.44%. It is shown that  $\epsilon_1$  and  $\epsilon_2$  are similar in values, but  $\epsilon_3$  is smaller than the other errors. These

errors might be associated with the assumed simple function of the optical gain response of SOE or POE and one-diode model adopted.

The errors in the short circuit current are  $-1.07$ ,  $6.54$  and  $-5.74\%$  for the cell without any optical elements, with SOE only, and with both SOE and POE, respectively, but the errors in the open circuit voltage are as small as  $0.51$ ,  $-0.10$  and  $-0.55\%$  for the cell. These errors are defined as the difference of the short circuit current or open circuit voltage predicted by the model from the corresponding experimental value, then divided by the experimental value and multiplied by 100%.

Compared with the optical intensity gain coefficient  $m = (0.50-0.86)$  for CCPCs shown in Table 4, SOE or POE seems to have a larger gain coefficient (0.92), suggesting that the cells are subject to a

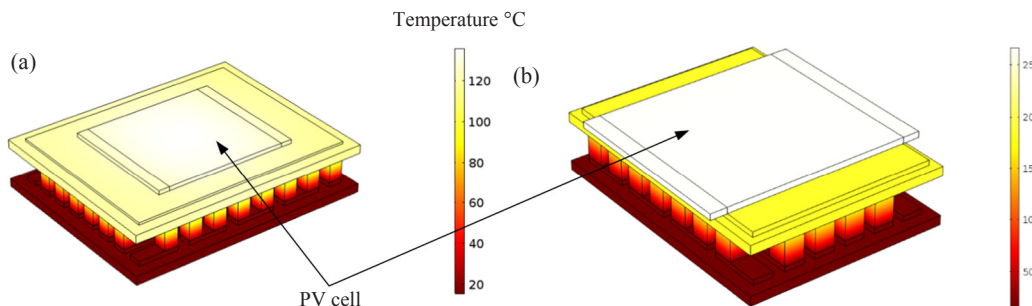


Fig. 11. Modelled temperature distribution of the PV cell and unpowered TE module under x300 optical concentration for (a) Type A and (b) Type B and C designs.

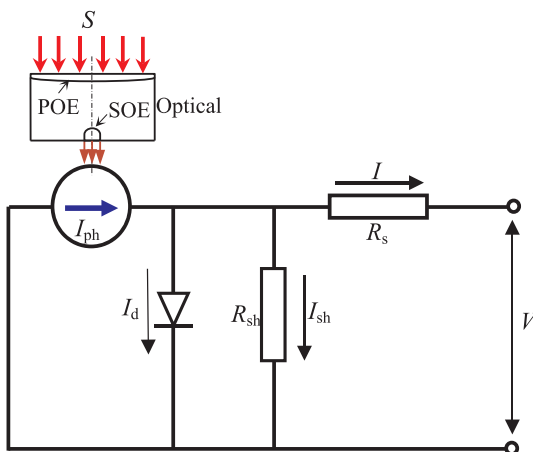


Fig. 12. Sketch of a lumped single-diode equivalent electrical circuit of the CPV cell with POE and SOE optics.

better optical efficiency. The values of  $I_d$ ,  $R_s$  and  $R_{sh}$  don't show a significant difference from those for monocrystalline PV cell/modules.

5. Discussion

Hybrid CPV-TE receivers have been designed, developed, manufactured and characterized experimentally and theoretically in this work. The TE module geometry has been simulated and improved for higher thermal conductivity. The critical thermal interfaces between the cell and TE module have also been improved. The PCB design has been upgraded with calibration marks for SOE attachment together with tracks to minimize hot-spot formation. Two cells from two different triple-junction CPV wafers with very similar experimental probe data were selected for receiver manufacture (Kappa and #13  $I_{sc}$  of 4.47 mA vs 4.48 mA,  $V_{oc}$  2.26 V vs 2.19 V at 1-sun.  $I_{sc}$  1.53A vs 1.46A,  $V_{oc}$  2.80 V vs 2.81 V, fill factor 82% for both, cell efficiencies 33.8% vs 34.1% respectively under 330-suns). The receivers were manufactured using two different TE module geometries (type A and type B). The optical alignment of the type B receiver is an improvement on type A. This is inferred from the concentration ratios calculated from the  $I_{sc}$

measurements, x371 for Kappa and x375 for #13. Improvement in optical alignment and higher CR caused a higher cell temperature for #13 than for Kappa, in the order of 30 °C based on  $V_{oc}$  measurements (3.1 V vs 3.0 V). The next step in this research will be to compare the performance of the thermoelectric modules, together with the CPV cell performance within type A and type B receivers. Identical thermal designs and optical concentration will be used to directly compare experimental results with the COMSOL model developed.

In the paper, we have extended previous work in [28] for monocrystalline PV cells/modules with CCPCs under a lower CR. The parameters in the six-parameter one-diode equivalent electrical model in [28] were successfully extracted based on a set of experimental  $I$ - $V$  curves of a triple-junction type A CPV-TE receiver with bare cell, SOE and POE optical elements respectively. The models show a satisfactorily small error in current. The results in this paper confirm that the six-parameter electrical model is applicable for triple-junction PV cells/modules with optical concentrating elements at a higher CR. In this paper, a simple electrical model for a whole III:V multi-junction cell was used, limiting the information obtained about the electrical performance of three component sub-cells. Future work will investigate complex photon quantum calculation combined with a parameter extracting procedure proposed in [30]. This will disclose the electrical performance of the component sub-cells. As a long-term research aim, the scaling law which involves outdoor conditions such as [31] will also be investigated.

6. Conclusions

Novel hybrid CPV-TE receiver designs were manufactured and electrically, thermally and theoretically analyzed under secondary and primary optical concentration. Accurate optical alignment of both SOE and POE to the cell were found to be a critical factor in the current-voltage characteristics measured. Additionally, the receiver-case thermal interface and rear heat sink designs were also key to the CPV-TE hybrid module for both CPV cell and TE cooling performance. The integrated TE module successfully acted as both a temperature sensor and as a solid-state heat pump for the CPV cell, enabling characterization of the cell in 5 °C operational temperature steps. The experimental platform enabled accurate measurement of electrical

Table 4  
The range of six parameters during optimization and the values extracted.

Parameter	$m$	$n$	$I_{ph0}$ (A)	$I_d$ (A)	$R_s$ ( $\Omega$ )	$R_{sh}$ ( $\Omega$ )
Range	[0, 1]	[0, 10]	[0, 10 <sup>-2</sup> ]	[0, 10 <sup>-7</sup> ]	[0, 0.1]	[0, 6000]
Extracted values	0.9171	4.2378	3.9564 × 10 <sup>-3</sup>	7.9030 × 10 <sup>-11</sup>	8.8647 × 10 <sup>-2</sup>	6000
Monocrystalline cell with 1 CCPC *	0.8611	1.101	2.8415 × 10 <sup>-2</sup>	1.6260 × 10 <sup>-11</sup>	4.5373 × 10 <sup>-1</sup>	6157.3
Monocrystalline module with 2 × 2 CCPC*	0.8234	3.1642	4.1385	1.3228 × 10 <sup>-6</sup>	1.6300 × 10 <sup>-2</sup>	1292.5
Monocrystalline module with 9 × 9 CCPC*	0.5099	10.015	4.4898 × 10 <sup>-1</sup>	4.7592 × 10 <sup>-10</sup>	3.5010 × 10 <sup>-2</sup>	6998.9
$\epsilon_1, \epsilon_2, \epsilon_3$ and $\epsilon$ (%)	5.24 (bare), 5.00 (SOE), 3.09 (POE), 4.44 (arithmetic mean)					
Error in short circuit current (%)	-1.07 (bare), 6.53 (SOE), -5.74 (POE)					
Error in open circuit voltage (%)	0.51 (bare), -0.10 (SOE), -0.55(POE)					

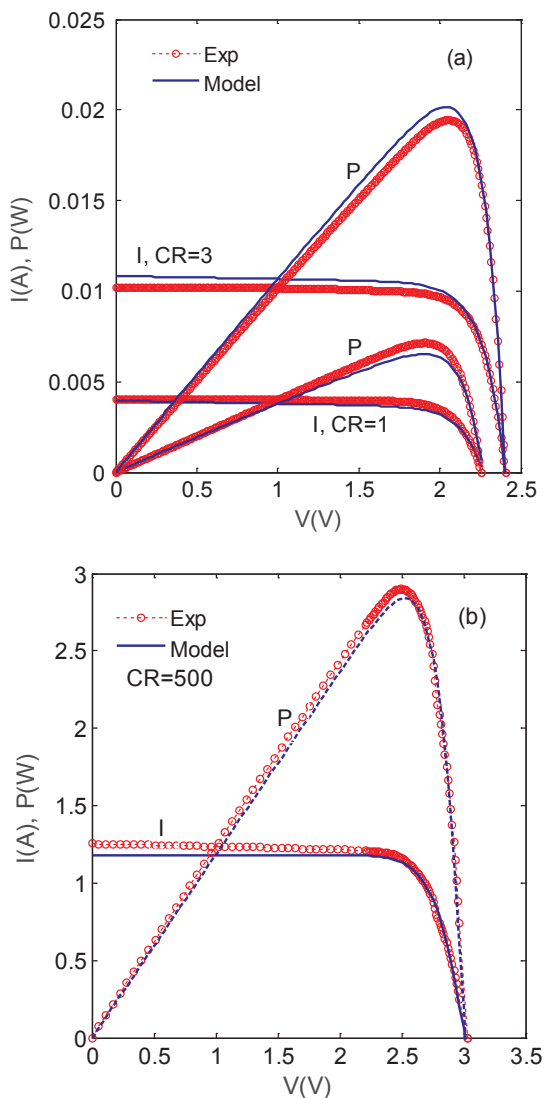


Fig. 13. A comparison of experimental  $I$ - $V$  curves of type A receivers with those predicted with model Eq. (1) and extracted parameters.

current-voltage characteristics under standard test conditions ( $1000 \text{ W/m}^2$  irradiance,  $25^\circ \text{C}$  temperature and AM1.5D spectrum) and elevated temperatures, with linear temperature coefficients obtained over the  $75^\circ \text{C}$  range tested.

A six-parameter single-diode equivalent electrical model was proposed for the multi-junction PV cells/modules and validated with the measured  $I$ - $V$  curves of type A PV module at concentration ratios 1, 3 and 500 under the standard test condition based on an optimization method in MATLAB. The determined six model parameters have been compared with those of monocrystalline PV cells/modules with CCPCs. The model can fit the experimental  $I$ - $V$  curves with a mean error of 4.44%, and the optical intensity gain coefficient of SOE and POE is very high, 0.92 in comparison with 0.50–0.86 for CCPCs. The extracted  $I_d$ ,  $R_s$  and  $R_{sh}$  values do not exhibit a considerable difference from those for monocrystalline PV cell/modules. The model can be used in multi-junction PV module development in the future. Further work includes sub-cells performance parameter identification for multi-junction PV modules with both SOE and POE. Photon quantum calculation in terms of solar spectrum and experimental  $I$ - $V$  curves, and the scaling law development for outdoor conditions will be developed. The experimental and theoretical work presented in this paper can be used for further thermally-dependant CPV cell characterization (both STC and non-STC) conditions. This data will be used for future hybrid CPV-TE

device architectures to optimize electrical performance and device/system lifetime whilst minimizing levelised cost of energy at system level.

## Acknowledgements

Sêr Cymru National Research Network and the EPSRC Solar Challenge project SUNTRAP (EP/K022156/1) are gratefully acknowledged for financial support, in addition to Innovate UK (project 102900). IQE plc are gratefully acknowledged for the supply of high efficiency III-V triple-junction CPV cells, and European Thermodynamics for Thermoelectric module supply. Cardiff University School of Physics are gratefully acknowledged for the use of cleanroom facilities.

## References

- [1] Current status of Concentrator Photovoltaic (CPV) technology Fraunhofer ISE and US DoE v1.3 < <https://www.ise.fraunhofer.de/content/dam/ise/de/documents/publications/studies/cpv-report-ise-nrel.pdf> > [Accessed 10/07/17].
- [2] Solargis solar resource map for direct normal irradiation published by the World Bank Group, funded by ESMAP < <http://globalsolaratlas.info> > [Accessed online 11/05/18].
- [3] Green MA, Emery K, Hishikawa Y, Warta W, Dunlop ED. Solar cell efficiency tables (version 47). Prog Photovolt Res Appl 2016;24(1):3–11.
- [4] Dimroth F, Tibbits TND, Niemeyer M, et al. Four-junction wafer-bonded concentrator solar cells. IEEE J Photovolt 2016;6(1):343–9.
- [5] Lumb M et al. 43rd PVSEC 2016 < <http://www.pvsec-26.com/pvsec-2016-singapore> > .
- [6] Ekins-Daukes NJ, Sandwell P, Nelson J, et al. What does CPV need to achieve in order to succeed? AIP Conf Proc 2016;1766(1):020004.
- [7] Sark WGHMV. Feasibility of photovoltaic – thermoelectric hybrid modules. Appl Energy 2011;88(8):2785–90.
- [8] Xu X, Zhou S, Meyers MM, et al. Performance analysis of a combination system of concentrating photovoltaic/thermal collector and thermoelectric generators. J Electron Pack 2014;136(4). 041004-041004.
- [9] Cui T, Xuan Y, Li Q. Design of a novel concentrating photovoltaic–thermoelectric system incorporated with phase change materials. Energy Convers Manage 2016;112:49–60.
- [10] Beeri O, Rotem O, Hazan E, et al. Hybrid photovoltaic-thermoelectric system for concentrated solar energy conversion: experimental realization and modeling. J Appl Phys 2015;118(11):115104.
- [11] James LW. Sandia National Laboratories Albuquerque, New Mexico for US Department of Energy (SAND89-7029); 1989.
- [12] Sweet TKN, Rolley M, Min G, et al. Scalable solar thermoelectric and photovoltaics (SUNTRAP). Am Inst Phys 2016;1766:080007.
- [13] Rolley M, Sweet T, Gao M. Novel photovoltaic-thermoelectric temperature control using a Closed-Loop Integrated Cooler (CLIC). IET Optoelectron 2017. <http://dx.doi.org/10.1049/iet-opt.2017.0072>.
- [14] Sweet TKN, Rolley MH, Prest MJ, Min G. Novel hybrid III-V concentrator photovoltaic-thermoelectric receiver designs. In: AIP Conference Proceedings; 2017. Vol. 1881. p. 080009.
- [15] Fernández EF, Ferrer-Rodríguez JP, Almonacid F, Pérez-Higueras P. Current-voltage dynamics of multi-junction CPV modules under different irradiance levels. Sol Energy 2017;155:39–50.
- [16] Theristis M, Fernández EF, Almonacid F, Pérez-Higueras P. Spectral corrections based on air mass, aerosole optical depth and precipitable water for CPV performance modelling. IEEE J Photovoltaics 2016;6(6).
- [17] Rodrigo PM, Fernández EF, Theristis M, Almonacid FC. Characterisation of the spectral matching ratio and the Z-parameter from atmospheric variables for CPV spectral evaluation. IEEE J Photovoltaics 2017;7(6).
- [18] Cotal H, Fetzer C, Boisvert J, Kinsey G, King R, Hebert P, et al. III-V multijunction solar cells for concentrating photovoltaics. Energy Environ Sci 2009;2:174–92.
- [19] Dominguez C, Anton I, Sala G. Multijunction solar cell model for translating I-V characteristics as a function of irradiance, spectrum, and cell temperature. Prog Photovoltaics Res Appl 2010;18:272–84.
- [20] Theristis M, O'Donovan TS. Electrical-thermal analysis of III-V triple-junction solar cells under variable spectra and ambient temperatures. Sol Energy 2015;118:533–46.
- [21] Theristis M, Fernández EF, Stark C, O'Donovan TS. A theoretical analysis of the impact of atmospheric parameters on the spectral, electrical and thermal performance of a concentrating III-V triple-junction solar cell. Energy Convers Manage 2016;117:218–27.
- [22] Segev G, Mittelman G, Kribus A. Equivalent circuit models for triple-junction concentrator solar cells. Sol Energy Mater Sol Cells 2012;98:57–65.
- [23] Lv H, Sheng F, Dai J, Liu W, Cheng C, Zhang J. Temperature-dependent model of concentrator photovoltaic modules combining optical elements and III-V multi-junction solar cells. Sol Energy 2015;112:351–60.
- [24] Or AB, Appelbaum J. Performance analysis of concentrator photovoltaic dense-array under non-uniform irradiance. Sol Energy Mater Sol Cells 2013;117:110–9.

- [25] Or AB, Appelbaum J. Estimation of multi-junction solar cell parameters. *Prog Photovoltaics Res Appl* 2013;21:713–23.
- [26] Helmers H, Schachtner M and Bett AW. Investigation on the influence of temperature and concentration on solar cell performances. In: Proceedings of 9th international conference on concentrator photovoltaic systems; 2013. p. 114–8.
- [27] Cooper T, Pravettoni M, Cadruvi M, Ambrosetti G, Steinfeld A. The effect of irradiance mismatch on a semi-dense array of triple-junction concentrator cells. *Sol Energy Mater Sol Cells* 2013;116:238–51.
- [28] Li W, Paul MC, Sellami N, Sweet TKN, Mallick TK, Gao M, et al. A six-parameter model of photovoltaic cell/module with crossed compound parabolic concentrator. *Sol Energy* 2016;137:551–63.
- [29] Anonymous. Optimization Toolbox™-User's Guide. The MathWorks, Inc., MA 01760-2098, USA; 2015.
- [30] Sweet TKN, Rolley MH, Li W, Paul MC, Johnson A, Davies JI, Tuleyd R, Simpson K, Ferrer-Rodríguez JP, Fernández EF, Knox AR. Multi-physics simulation and experimental characterization of hybrid III:V concentrator photovoltaic-thermoelectric receiver designs under primary and secondary optical elements. In: 9th International Conference on Applied Energy, ICAE2017, 21–24 August 2017, Cardiff, UK; 2017.
- [31] Li W, Paul MC, Rolley M, Sweet T, Siviter J, Baig H, et al. A scaling law for monocrystalline PV/T modules with CCPC and comparison with triple junction PV cells. *Appl Energy* 2017;202:755–71.